





Cite this: *Environ. Sci.: Adv.*, 2022, 1, 530

## Aqueous ibuprofen sorption by using activated walnut shell biochar: process optimization and cost estimation†

Manvendra Patel, <sup>a</sup> Abhishek Kumar Chaubey,<sup>a</sup> Charles U. Pittman, Jr.<sup>b</sup> and Dinesh Mohan <sup>\*a</sup>

Ibuprofen is a widely used non-steroidal anti-inflammatory, anti-pyritic, and analgesic drug with occurrence in the aquatic systems of 47 countries. The presence of ibuprofen in aquatic systems poses a threat to flora and fauna. Therefore, this study developed walnut shell activated biochar (WSAB) using  $\text{H}_3\text{PO}_4$  immersion and 450 °C pyrolysis as a 3-dimensional adsorbent for aqueous ibuprofen remediation. WSAB was characterized using elemental analysis, ATR-FTIR, XRD, SEM, SEM-EDX, TEM, BET surface area and pore size measurements. The  $S_{\text{BET}}$  surface area, pore volume, and pore density of the WSAB were  $686 \text{ m}^2 \text{ g}^{-1}$ ,  $0.38 \text{ cm}^3 \text{ g}^{-1}$  and  $0.87 \text{ g cm}^{-3}$ , respectively. Batch sorption studies were performed from pH 2 to 10 at ibuprofen concentrations from 10 to 120  $\text{mg L}^{-1}$  and temperatures from 25 to 45 °C. Maximum sorption (80%) occurred at pH 4 at an IBP concentration of 50  $\text{mg L}^{-1}$  and a WSAB dose of 1.0  $\text{g L}^{-1}$ . Sorption followed second order kinetics well ( $R^2 = 0.999$ ). The sorption isotherms remained almost constant with an increase in temperature as shown by Langmuir adsorption capacities [ $Q^{\circ}_{25^{\circ}\text{C}} = 69.7 \text{ mg g}^{-1}$ ,  $Q^{\circ}_{35^{\circ}\text{C}} = 68.0 \text{ mg g}^{-1}$ , and  $Q^{\circ}_{45^{\circ}\text{C}} = 66.9 \text{ mg g}^{-1}$ ]. WSAB provided an efficient ibuprofen sorption capacity ( $30.08 \text{ mg g}^{-1}$ ) in fixed-bed sorption studies (column parameters: initial Ibuprofen concentration = 7.5  $\text{mg L}^{-1}$ ; pH = 4.0; WSAB dose = 2.0 g; bed length = ~4 cm; hydraulic flow rate = 2.5  $\text{mL min}^{-1}$ ). Sorption of ibuprofen to WSAB involves H-bonding, pore filling with complexation and hydrophobic  $\pi$ - $\pi$  donor-acceptor attractions likely participating. An estimated cost of US\$ 6.93  $\text{kg}^{-1}$  together with excellent sorption capacity makes WSAB an efficient low-cost adsorbent for ibuprofen removal. Thus, this study describes a sustainable waste walnut shell management strategy as well as treatment of ibuprofen contaminated water.

Received 22nd January 2022  
Accepted 4th July 2022

DOI: 10.1039/d2va00015f

rsc.li/esadvances

### Environmental significance

The widely used, non-steroidal anti-inflammatory, anti-pyritic, and analgesic drug, ibuprofen, has been chosen as the model for pharmaceutical removal owing to its worldwide presence in aquatic systems. Thus, walnut shell activated biochar (WSAB) was prepared as a 3-D adsorbent for aqueous ibuprofen remediation. The ability of the engineered biochar to treat ibuprofen from natural water samples was successfully demonstrated. For the first time, in-depth mechanisms including hydrogen bond formation and  $\pi$ - $\pi$  donor-acceptor and electrostatic interactions were explored and demonstrated using chemical reactions for ibuprofen removal. Sorption efficiency of WSAB has a higher ibuprofen sorption than most biochars/adsorbents so far reported. Thus, this study provides sustainable waste walnut shell management as well as ibuprofen contaminated water treatment.

## 1. Introduction

Pharmaceuticals are a very important and widely discarded class of chemicals used daily worldwide. Pharmaceuticals have rapidly become an emerging class of contaminants due to their continuous use.<sup>1,2</sup> During the last 2 decades, the presence of

pharmaceuticals in the environment has increased enormously.<sup>2-5</sup> Pharmaceutical manufacturing effluents contain high quantities of pharmaceutical residues up to the 100  $\mu\text{g L}^{-1}$  level.<sup>2,6-9</sup> Continuous manufacturing site discharges, human and veterinary usage, disposal and excretion caused this increase in aquatic pharmaceutical pollution.<sup>2,5</sup> The most common pharmaceutical categories that contaminate aqueous systems are anti-inflammatories, analgesics, antidepressants, antiepileptics, antibiotics, antacids, antipyretics, beta-blockers, tranquillizers, and steroids.<sup>2,10</sup> Ibuprofen is a non-steroidal anti-inflammatory drug (NSAID) with analgesic and antipyretic properties. It is widely used for fever, pain, inflammatory

<sup>a</sup>School of Environmental Sciences, Jawaharlal Nehru University, New Delhi, 110067, India. E-mail: dm\_1967@hotmail.com; Fax: +91-11-26704616; Tel: +91-11-26704616

<sup>b</sup>Department of Chemistry, Mississippi State University, Mississippi, MS 39762-149573, USA

† Electronic supplementary information (ESI) available. See <https://doi.org/10.1039/d2va00015f>



problems and rheumatic disorders. Ibuprofen is one of the most commonly used and consumed pharmaceuticals and has a high mobility in aquatic environment systems.<sup>1,5,11</sup> To date, ibuprofen has been reported in the waterways of 47 countries<sup>4</sup> and undoubtedly exists in far more.

Conventional wastewater treatment plants are unable to remove pharmaceuticals completely, leading to their presence in rivers, lakes, streams and oceans.<sup>12</sup> Advanced treatments used to remediate pharmaceuticals include ozonation, photolysis, Fenton oxidation, electrochemical degradation, ultrasound irradiation and membrane filtration. However, these methods are cost-intensive and generate toxic transformation products and sludge.<sup>2,5</sup> In contrast, adsorption is suitable for pharmaceutical removal from aquatic systems as it is economical and does not generate toxic products.<sup>13</sup> Activated carbon, biochar, nanocomposites and mesoporous silica adsorbents have been used by many researchers for the pharmaceutical adsorption.<sup>11,13–17</sup> We now describe a low-cost and sustainable walnut shell-activated biochar and its successful use for aqueous ibuprofen uptake. Global walnut production exceeded 3.8 million tons in 2017.<sup>18</sup> Walnut shells comprise ~67% of the total mass. About 2.5 million tons of walnut shells were produced in 2017. In India, 299 710 tons of walnuts were produced in 2017.<sup>19</sup>

The large production of these shells with little use (except for burning which causes air pollution) makes walnut shells a perfect precursor for biochar development.<sup>18,19</sup> Thus, walnut shell use for activated biochar development followed by ibuprofen removal proves to be a “double edged sword” for environmental protection where both edges are useful.

We now describe a low-cost and sustainable walnut shell-activated biochar and its successful use for aqueous ibuprofen uptake. Ibuprofen sorption interactions with WSAB are proposed and discussed in detail. A walnut shell activated biochar cost estimate was developed. Usually, the literature reports batch removal studies for pharmaceuticals, while column studies of pharmaceutical sorption are far less common. Thus, both batch sorption studies and fixed-bed column studies were conducted in this study. Batch studies have several advantages including ease of obtaining variables/parameter estimates at the lab scale. However, batch sorption parameters are not completely applicable for large scale treatment operations due to different solid-to-liquid ratios, contact kinetics, hydrodynamic factors, *etc.*<sup>20,21</sup> Thus, batch sorption studies accompanied by column operations provide a better understanding of sorption. The fixed-bed data were also fitted by the Adams–Bohart and Thomas models. Thus, this study provides a good starting point for a more detailed development of walnut shell activated biochar for aqueous ibuprofen removal. The main objective of this study was to develop activated walnut shell biochar for aqueous ibuprofen removal. Kinetic and isotherm studies were undertaken to optimize the pH, initial ibuprofen concentration, WSAB dose, and temperature for ibuprofen sorption. The obtained column parameters will be useful for implementing this adsorbent for commercial scale applications.

## 2. Materials and methods

### 2.1. Apparatus and reagents

Analytical grade chemicals were used in this study. ( $\pm$ ) Ibuprofen [2-(4-isobutylphenyl)propionic acid]; purity 98%, M.W. 206.28 was procured from Calbiochem, an affiliate of Merck KGaA, Darmstadt, Germany. All reagents used were weighed using a Mettler Toledo balance (model AB 265-S/FACT). pH measurements employed a Thermo Scientific pH meter (model Orion 5 Star). The pH adjustments were made with 0.1 N HCl and 0.1 N NaOH. Batch adsorptions were performed in a temperature-controlled water bath shaker (model Scientech India). Ibuprofen solutions were prepared fresh for all experiments (details in ESI section S1†). Ibuprofen concentrations were determined by using a UV/Vis spectrophotometer (model Lambda 35, PerkinElmer) at a  $\lambda_{\text{max}}$  of 264 nm. Nylon syringe filters (0.2  $\mu\text{m}$ , SY25NN, MDI India) were used to filter the samples.

### 2.2. Development of walnut shell activated biochar

Walnut shell activated biochar (WSAB) was prepared by acid activation as reported previously for activated carbon.<sup>22</sup> Walnut shells were soaked in 50%  $\text{H}_3\text{PO}_4$  at 1 : 1 (w/w) solution for 24 h at room temperature. These shells (500 g per batch) were pyrolyzed in a muffle furnace under  $\text{N}_2$  (flow rate =  $0.1 \text{ m}^3 \text{ h}^{-1}$ ) and heated initially to 170 °C for 0.5 h. Then, the pyrolysis temperature was increased to 450 °C, held for 1 h and cooled under a  $\text{N}_2$  flow. The activated biochar obtained was washed multiple times with DDW until the biochar pH is stabilized (~7.0). Then WSAB was dried for 24 h at 100 °C, sieved into different mesh size fractions (>50, 50–100, 100–150, 150–200, and 200–300) and stored in air-tight containers for further use. The 100–150 mesh (150 to 106  $\mu\text{m}$ ) WSAB was used for both batch and fixed-bed sorption studies.

### 2.3. Characterization of activated biochar (WSAB)

A Quantachrome Autosorb-1 surface area analyzer was used to obtain the  $\text{N}_2$  adsorption isotherms. WSAB (0.15 g) was out-gassed at 250 °C for 12 h at  $<10^{-3}$  Torr. The specific surface area ( $S_{\text{BET}}$ ) was evaluated as reported elsewhere.<sup>22</sup> The density measurements were performed using a Quantachrome Stereopycnometer as reported previously.<sup>22</sup>  $\text{pH}_{\text{zpc}}$  of the WSAB was estimated as previously reported.<sup>17</sup> Ash content of WSAB was evaluated according to the ASTM method D-1762-84.<sup>23,24</sup> The WSAB elemental composition was determined by an acid-digestion method (EPA method 3052) and analyzed using ICP. XRF (PANalytical Epsilon 5) was also used for elemental composition analysis by preparing WSAB pellets.

SEM and TEM analyses were used to probe WSAB's surface morphologies. SEM analysis was performed by employing a Zeiss EVO40 SEM (accelerating voltage 20 000 volts; working distance 10 000–10 500  $\mu\text{m}$ ). SEM WSAB samples were mounted on a stainless steel stub using a double stick carbon tape and coated under vacuum with gold. EDX analysis was performed to determine the surface elemental composition (to a 2  $\mu\text{m}$  depth). Energy dispersive analysis was carried out with



a Bruker EDX system fitted to the Zeiss EVO40 SEM. WSAB was dispersed in ethanol for TEM analysis followed by 10 min ultra-sonication and fixing on a carbon-coated copper grid. TEM images were recorded with a JEOL JEM 2100F (Japan) operated at 200 KeV.

An ATR-FTIR spectrometer (model FRONTIER, PerkinElmer) was used to record the ATR-FTIR spectra of WSAB samples from 4000 to 600  $\text{cm}^{-1}$ . Walnut shell activated biochar samples were directly analyzed by placing a few mg of the sample in the ATR-FTIR spectrometer. A PANalytical X-ray Diffractometer model X'Pert PRO was used to identify mineral content and crystallinity in WSAB using  $\text{Cu-K}\alpha$  ( $\lambda = 1.54 \text{ \AA}$ ) radiation at 45 kV and 40 mA at a scanning speed of  $2^\circ \text{ min}^{-1}$  from  $10^\circ$  to  $90^\circ$ .

#### 2.4. Batch sorption studies

Batch sorption studies were used for equilibrium, kinetic and pH sorption studies. The pH for optimum ibuprofen adsorption was determined from pH 2 to 10 using 0.05 L of 50  $\text{mg L}^{-1}$  aqueous ibuprofen with 0.05 g WSAB doses. The samples were agitated for 24 h in a temperature-controlled water bath shaker at a constant speed of 120 rpm. The solutions were then filtered using 0.2  $\mu\text{m}$  syringe filters and analyzed for post-sorption ibuprofen concentration. The amount of ibuprofen sorbed onto WSAB was estimated using eqn (1).

$$Q_e = (C_o - C_e)V/W \quad (1)$$

Here,  $C_o$  and  $C_e$  are initial and equilibrium ibuprofen concentrations in  $\text{mg L}^{-1}$ ;  $V$  is the volume of ibuprofen solution used in liters;  $W$  is the amount of WSAB in grams.

Kinetic studies examined the effect of the contact time, WSAB dose and ibuprofen concentrations on sorption. WSAB doses (0.5, 1.0 and 2.0  $\text{g L}^{-1}$ ) were used to determine the effects of adsorbent dose on kinetics and the optimum dose for ibuprofen adsorption. The initial ibuprofen concentration effect on the rate was evaluated at 25, 50, and 100  $\text{mg L}^{-1}$ . This kinetic data were fitted to pseudo-first order<sup>25</sup> and pseudo-second order<sup>26</sup> rate equations (summarized in Table S1†). All kinetic and sorption equilibrium studies were carried out at an optimum pH of 4.0.

Sorption isotherm studies were performed at 25, 35 and 45  $^\circ\text{C}$  over the 10–120  $\text{mg L}^{-1}$  ibuprofen concentration range. This concentration range was higher than environmental concentrations and was used to estimate the adsorbent effectiveness and to evaluate its maximum adsorbent capacity. The isotherm data were fitted into Freundlich<sup>27</sup> and Langmuir<sup>28</sup> isotherm models. The equations and their parameters are listed in Table S1.†

#### 2.5. Column studies

Fixed bed studies are important in industrial contaminant removal applications.<sup>29</sup> Design parameters obtained from fixed bed column studies can easily be utilized for large scale commercial applications. Thus, fixed bed column studies were performed as reported previously.<sup>29–39</sup> The fixed bed column was

operated under gravity in the down flow mode with glass wool as the column support. A distilled water slurry of 2 g WSAB (100–150 mesh BSS mesh) was fed slowly into an acrylic column (diameter = 2 cm; length = 40 cm). The adsorption column bed length was  $\sim 4$  cm, and a hydraulic flow rate of 2.5  $\text{mL min}^{-1}$  was maintained. An ibuprofen solution ( $7.5 \text{ mg L}^{-1}$ ) eluted through the WSAB-loaded column. An effluent sample was collected and analyzed every 30 min. Column parameters including breakpoint and exhaustion capacity, breakpoint and exhaustion volume, percent saturation and empty-bed-contact-time (EBCT) were calculated.<sup>30,31,33,34,36,37</sup>

Weber's mass transfer model was used for designing the fixed-bed adsorption column.<sup>29</sup> The expression of an ideal breakthrough curve in terms of ibuprofen effluent concentration ( $C_f$ ) and total ibuprofen-free water mass ( $\overline{V_e}$ ) passing through WSAB's per unit cross sectional area depends upon:

(i) Total ibuprofen effluent mass per unit WSAB area at breakpoint ( $\overline{V_b}$ ) and

(ii) Curve's nature between ( $\overline{V_b}$ ) and ( $\overline{V_x}$ ) where ( $\overline{V_x}$ ) is total ibuprofen effluent's mass per unit WSAB area, when WSAB is approaching towards the saturation. ( $C_b$ ) and ( $C_x$ ) are the ibuprofen effluent concentrations at ( $\overline{V_b}$ ) and ( $\overline{V_x}$ ), respectively. The constant zone length ( $\delta$ ) is the part of the WSAB bed, when the ibuprofen concentration decreased from ( $C_b$ ) and ( $C_x$ ). All parameters of this mass transfer model are shown in eqn (2)–(10) below.

$$\text{The total time taken by primary adsorption zone} = t_x = \frac{\overline{V_x}}{F_m} \quad (2)$$

where ( $F_m$ ) is the mass flow rate which is defined as the mass per unit cross-sectional area of the bed.

The time ( $t_\delta$ ) required for the primary adsorption zone (PAZ) to move down to its own length in the glass column

$$t_\delta = \frac{\overline{V_x} - \overline{V_b}}{F_m} \quad (3)$$

$$\text{The ratio of WSAB bed depth}(D)\text{to the time} = \frac{\delta}{D} = \frac{t_\delta}{t_x - t_b} \quad (4)$$

where  $t_b$  and  $t_x$  are time duration up to the breakpoint and exhaustion point (in mins), respectively

$$\text{The fractional capacity} = f = 1 - \frac{t_b}{t_\delta} \quad (5)$$

The length of the PAZ ( $\delta$ )

$$\delta = D \left[ \frac{t_\delta}{t_b + t_\delta(f - 1)} \right] \quad (6)$$

where  $D$  is the biochar bed depth.

The percent saturation is determined using eqn (7).

$$\text{Percent saturation} = \frac{D - \delta(f)}{D} \times 100 \quad (7)$$



The breakthrough capacity and the total column capacity were calculated by dividing the area between the effluent and influent to the breakthrough point and the total area under the breakthrough curve by the weight of the WSAB used. In addition, other parameters including the empty-bed-contact-time, bed volume, and WSAB usage rate are determined using eqn (8)–(10).<sup>29</sup>

$$\text{Bed volume} = \frac{\text{Weight of biochar(kg)}}{\text{Biochar bulk density} \left( \frac{\text{kg}}{\text{m}^3} \right)} \quad (8)$$

Empty bed contact time (EBCT)

$$\text{EBCT} = \frac{\text{Bed volume}}{\text{Flow rate}} \quad (9)$$

The biochar usage rate

$$\begin{aligned} &\text{Walnut shell activated biochar(WSAB)usage rate} \\ &= \frac{\text{Weight of biochar in column(g)}}{\text{Breakthrough volume(L)}} \quad (10) \end{aligned}$$

Further, Adams–Bohart<sup>40</sup> and Thomas<sup>41</sup> models were also applied to the dynamic sorption data. The Adams–Bohart model is used to describe the initial part of the breakthrough curve.<sup>40,42</sup> The Adams–Bohart model establishes the relationship between  $C_e/C_o$  and time ( $t$ ) in a dynamic system as shown in eqn (11). Here,

$$\ln \frac{C_e}{C_o} = K_{AB} C_o t - K_{AB} N_o \frac{Z}{F} \quad (11)$$

where  $C_o$  and  $C_e$  ( $\text{mg L}^{-1}$ ) are the influent and effluent ibuprofen concentrations,  $K_{AB}$  ( $\text{L mg}^{-1} \cdot \text{min}$ ) is the Adams–Bohart constant, and  $F$  ( $\text{cm min}^{-1}$ ) is the linear velocity.  $F$  is calculated by dividing the flow rate by the column cross section area.  $Z$  (cm) is the fixed-bed column's bed depth and  $N_o$  ( $\text{g L}^{-1}$ ) is the column's ibuprofen concentration at saturation. A linear plot of  $\ln(C_e/C_o)$  against time ( $t$ ) and the values of  $K_{AB}$  and  $N_o$  were determined from the intercept and slope of the curve (Fig. S6†).

The Thomas model uses second-order kinetics and the Langmuir isotherm for equilibrium.<sup>41</sup> The Thomas model assumes plug flow behavior in a fixed-bed and is suitable for sorption processes where external and internal diffusion limitations are absent.<sup>41,42</sup> Thomas model's linearized form is shown in eqn (12).

$$\ln \left( \frac{C_o}{C_e} - 1 \right) = \frac{K_{Th} q_o W}{Q} - K_{Th} C_o t \quad (12)$$

where  $K_{Th}$  ( $\text{mL min}^{-1} \text{mg}^{-1}$ ) is the Thomas rate constant,  $q_o$  ( $\text{g g}^{-1}$ ) is ibuprofen sorption capacity,  $C_o$  and  $C_e$  ( $\text{mg L}^{-1}$ ) are the influent and effluent ibuprofen concentrations,  $Q$  ( $\text{mL min}^{-1}$ ) is the flow rate,  $W$  (g) is the WSAB mass in the column and  $t$  (min) is the total flow time. The linear plot of  $\ln[(C_o/C_e) - 1]$  against time ( $t$ ) provides  $K_{Th}$  and  $q_o$  values from its intercept and slope (Fig. S7†).

## 2.6. Cost estimation

Cost estimation for adsorbent preparation is crucial for water treatment at a commercial scale.<sup>43,44</sup> Adsorbent feasibility depends, in part, upon its overall preparation cost. Adsorbent cost analysis becomes especially important in low and middle income countries.<sup>45</sup> Estimating adsorbent costs requires adding the preparation step's costs, including adsorbent precursor/raw material collection and processing (including cleaning, drying and size reduction), activation/modification, carbonization, washing and drying. Precursor availability, the number of treatments, processing required and electricity costs are important considerations.<sup>43,44</sup> Commercial adsorbent selection depends highly upon its preparation cost.<sup>45</sup> Few adsorbent cost estimates exist for pharmaceutical adsorptions.<sup>46,47</sup>

A possible approach to evaluate total adsorbent preparation cost (modified from previously reported methods by Chakraborty and colleagues)<sup>43,44</sup> is suggested and summarized below:

$$\text{COST}_{BC} = \text{COST}_P + \text{COST}_{Pro} + \text{COST}_{A/M} + \text{COST}_C + \text{OTHER COSTS}$$

where  $\text{COST}_{BC}$  = total cost of adsorbent preparation,  $\text{COST}_P$  = cost of precursor procurement,  $\text{COST}_{Pro}$  = cost incurred during precursor processing (including washing, drying, and sizing).  $\text{COST}_{A/M}$  = cost of chemicals used in biochar activation;  $\text{COST}_C$  = cost of biochar preparation, *i.e.* pyrolysis (mainly includes electricity cost for pyrolysis). OTHER COST includes costs incurred during the biochar preparation along with 10% offset costs for any mass loss occurred during the entire process. All costs were initially calculated in Indian rupee (₹). These were finally converted and reported in US\$ (1 US\$ = ₹ 79.62 as on August 15, 2022).

## 3. Results and discussion

### 3.1. Characterization of activated biochar

The surface area ( $S_{BET}$ ) of WSAB from the nitrogen adsorption-desorption isotherm (Fig. S1†) was  $686 \text{ m}^2 \text{ g}^{-1}$  (Table 1). The macro-, meso-, and micro-pore volumes of WSAB were 0.07, 0.12 and  $0.38 \text{ cm}^3 \text{ g}^{-1}$ , respectively (Table 1). The WSAB bulk density or apparent density was  $0.87 \text{ g cm}^{-3}$ ; however, its solid or skeletal density is  $1.04 \text{ g cm}^{-3}$  (Table 1). The WSAB ash content was 2.38% (Table 2). The  $\text{pH}_{ZPC}$  of WSAB was  $\sim 2.0$  (Table 2); thus at a pH above 2.0, WSAB becomes negatively charged. Proximate analysis showed carbon (45.0%) oxygen (45.34%) and hydrogen (6.25%) as the main constituents of the walnut shell activated biochar (Table 2). Elements were reported as oxides [ $\text{Al}_2\text{O}_3 = 1.08\%$ ;  $\text{SiO}_2 = 0.87\%$ ;  $\text{K}_2\text{O} = 0.20\%$ ;  $\text{Na}_2\text{O} = 0.28\%$ ;  $\text{CaO} = 0.15\%$ ;  $\text{Fe}_2\text{O}_3 = 0.17\%$ ] by convention in walnut shell activated biochar (Table 2). Chloride (Cl = 0.60%) and silica ( $\text{SiO}_2 = 0.87\%$ ) were determined through XRF analysis.

The surface morphology of WSAB from SEM imaging at different magnifications [Fig. 1a and b] exhibits an irregular surface morphology with both meso- and macro-porous structures. This correlates with the porosity data (Table 1). These structures give a large surface area ( $686 \text{ m}^2 \text{ g}^{-1}$ ), which enhanced ibuprofen sorption. The presence of surface carbon,



Table 1 Surface areas, pore volumes and densities of walnut shell activated biochar (WSAB)<sup>a</sup>

Sample	$S_{\text{BET}}$ ( $\text{m}^2 \text{g}^{-1}$ )	$V_{\text{ma-p}}$ ( $\text{cm}^3 \text{g}^{-1}$ )	$W_0$ ( $\text{cm}^3 \text{g}^{-1}$ )	$V_{\text{me-p}}$ ( $\text{cm}^3 \text{g}^{-1}$ )	$V_{\text{T}}$ ( $\text{cm}^3 \text{g}^{-1}$ )	$\rho_{\text{Hg}}$ ( $\text{g cm}^{-3}$ )	Skeletal density <sup>b</sup> ( $\text{g cm}^{-3}$ )	Apparent density ( $\text{g cm}^{-3}$ )	Bulk density ( $\text{g cm}^{-3}$ )
Walnut shell activated biochar (WSAB)	686	0.07	0.38	0.12	0.57	1.73	1.04	0.87	0.87

<sup>a</sup>  $\text{N}_2$  isotherm at  $-196^\circ\text{C}$ ;  $S_{\text{BET}}$  (the specific surface area, BET equation,  $p/p_0 = 0.05-0.35$ , and  $am = 16.2 \text{ \AA}^2$ ),  $W_0$  (micropore volume; the Dubinin-Radushkevich equation). Mercury porosimetry:  $V_{\text{me-p}}$  (mesopore volume),  $V_{\text{ma-p}}$  (macropore volume), density measurement:  $V_{\text{T}}$  (total pore volume) =  $1/\rho_{\text{Hg}} - 1/\rho_{\text{He}}$ ,  $\rho_{\text{He}}$  = helium density and  $\rho_{\text{Hg}}$  = mercury density. <sup>b</sup> Skeletal density: the ratio of the mass of biochar to the sum of the volumes of the biochar and closed pores within the material.

Table 2 Proximate and elemental analyses of the walnut shell activated biochar

Elements/compounds	Weight (%)
<b>Proximate analysis<sup>a</sup></b>	
Carbon	45.03
Hydrogen	6.25
Nitrogen	0.96
Sulfur	0.04
Oxygen	45.34
Ash content	2.38
$\text{pH}_{\text{ZPC}}$	~2.0
<b>Elemental analysis (reported as oxides by convention)<sup>b</sup></b>	
$\text{Al}_2\text{O}_3$	1.08
BaO	0.05
CaO	0.154
$\text{Fe}_2\text{O}_3$	0.172
$\text{K}_2\text{O}$	0.20
MgO	1206 ppm
$\text{Na}_2\text{O}$	0.27
$\text{SiO}_2^c$	0.87
SrO	0.04
$\text{TiO}_2$	0.28
$\text{Cl}^c$	0.60

<sup>a</sup> Ash content was determined by incinerating (air-treating) about 1 g of the sample at  $650^\circ\text{C}$  for 12 h in an electric furnace. <sup>b</sup> The samples were dissolved in lithium metaborate fusion and run on a PerkinElmer Optima 5300 ICP. <sup>c</sup> Estimated through XRF analysis.

silicon and oxygen on WSAB was confirmed by the SEM-EDX spectra (Fig. 1c). Since SEM-EDX only shows the surface (up to  $2-3 \mu\text{m}$ ) elemental content of the WSAB, the SEM-EDX results can differ with bulk elemental composition.<sup>48</sup> The TEM images presented in Fig. 1d-f also reveal the irregular shapes and amorphous nature of walnut shell activated biochar. The TEM images of WSAB show thin sheet-like structures.

WSAB peaks observed by ATR-FTIR (Fig. 2a) correspond to hydroxyl, lactones, and aromatic and aliphatic functional groups. The broad peak between  $3800$  and  $3500 \text{ cm}^{-1}$  corresponds to non H-bonded organic and possible inorganic -OH stretching.<sup>49-51</sup> Surface-bound water can also be present. The pair of peaks at  $2988$  and  $2905 \text{ cm}^{-1}$  belong to the asymmetric and symmetric stretching of  $\text{sp}^3$ -hybridized C-H groups in WSAB.<sup>51</sup> The  $1712 \text{ cm}^{-1}$  peak is due to C=O stretching.<sup>22,31</sup> The  $1560 \text{ cm}^{-1}$  peak is attributed to

conjugated aromatic ring breathing modes,<sup>31,49</sup> while that at  $1453 \text{ cm}^{-1}$  corresponds to  $-\text{CH}_2$  bending vibrations in the WSAB.<sup>51,52</sup> The peaks at  $1225 \text{ cm}^{-1}$ ,  $1160 \text{ cm}^{-1}$  and  $1060 \text{ cm}^{-1}$  correspond to aromatic and aliphatic ether C-O stretching vibrations in the activated biochar.<sup>51</sup> Sharp peaks at  $875$  and  $665 \text{ cm}^{-1}$  are assigned to out-of-plane C-H bending modes of the aryl ring.<sup>51</sup>

The WSAB XRD pattern (Fig. 2b) exhibits a single broad peak around  $2\theta = 24^\circ$ , representing the (0 0 2) graphitic basal plane reflections<sup>53</sup> of amorphous aromatic carbon.<sup>22</sup> This broad peak also exhibits a strong small angle scattering, indicating the amorphous nature of WSAB carbonaceous structures with high porosity.<sup>54,55</sup> Small broad peaks of (1 0 0) and (1 1 0) near  $42^\circ$  and  $79^\circ$  indicate that WSAB contains some small ordered graphene sheet domains.<sup>53</sup>

### 3.2. Sorption studies

**3.2.1. Kinetic studies and modeling.** WSAB dosage and initial ibuprofen concentration effects on adsorption are shown in Fig. S2 and S3,† respectively. A significant increase in the adsorption occurred (from 70 to ~98%) as WSAB dosage increased from  $0.5$  to  $2.0 \text{ g L}^{-1}$  (Fig. S2†). However, the percent ibuprofen removal declined with increase in the initial ibuprofen concentration from 25, 50 and  $100 \text{ mg L}^{-1}$  (Fig. S3†).

Pseudo-first order and pseudo-second order rate parameters for ibuprofen sorption on WSAB at different doses and concentrations are shown in Table 3. Pseudo-second order fits were far better with  $R^2$  values of 0.998, 0.999 and 0.999, respectively, for  $0.5$ ,  $1.0$  and  $2.0 \text{ g L}^{-1}$  WSAB doses. Also, second order correlations maintained high  $R^2 = 0.995$ , 0.999 and 0.997 for 25, 50 and  $100 \text{ mg L}^{-1}$  ibuprofen concentrations, respectively [Fig. 3a and b]. The linear pseudo-first order dose and concentration kinetic plots are given in Fig. S4.† Ibuprofen sorption equilibrium is achieved in less than 24 h (Fig. S3†). The maximum removal efficiency increases from 76.0% at  $0.5 \text{ g L}^{-1}$  WSAB dose to ~98% at  $2.0 \text{ g L}^{-1}$  WSAB dose at  $50 \text{ mg L}^{-1}$  ibuprofen concentration. The maximum removal efficiency also increased with a drop in the ibuprofen concentration. The removal efficiency at  $1.0 \text{ g L}^{-1}$  WSAB dose increased from 63.0 to 100% as the ibuprofen concentration dropped from 100 to  $25 \text{ mg L}^{-1}$ .

**3.2.2. Sorption isotherms and modeling.** The batch sorption isotherm data, obtained at 25, 35 and  $45^\circ\text{C}$  at an optimum adsorbent dose of  $1.0 \text{ g L}^{-1}$  (Fig. S5†), were fitted to Freundlich



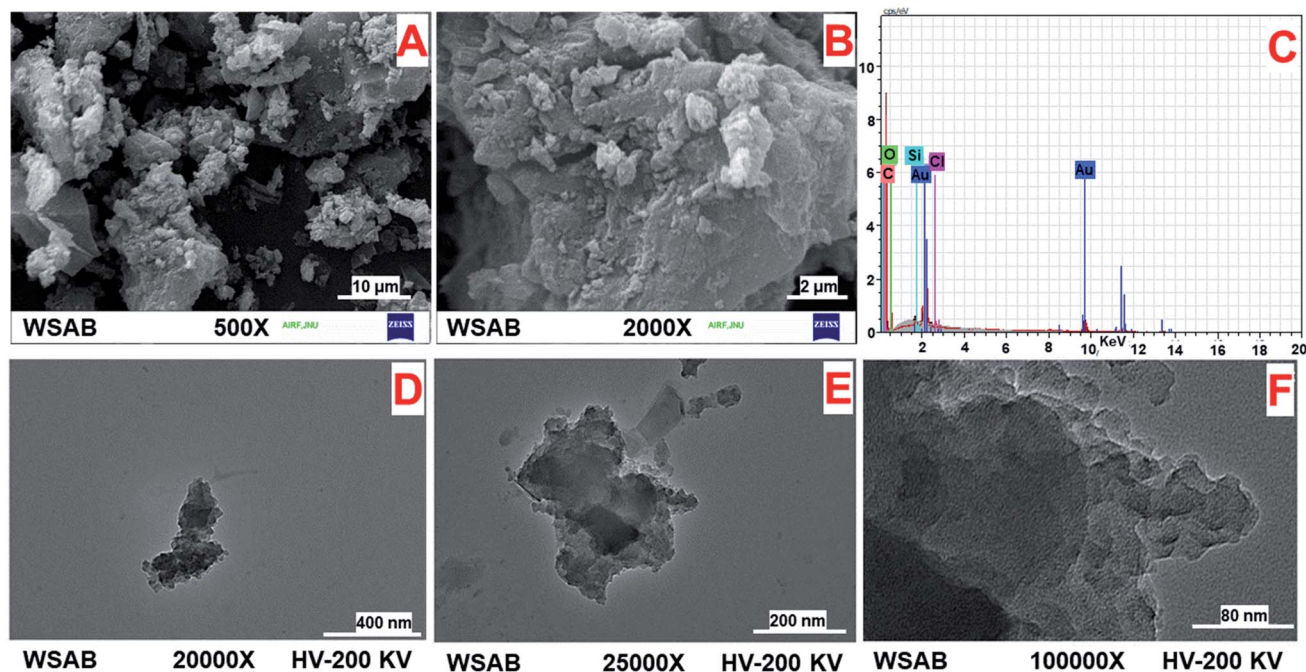


Fig. 1 SEM micrographs (A) at 500 $\times$  and (B) at 2000 $\times$ , (C) SEM-EDX spectra, and (D–F) TEM micrographs of WSAB.

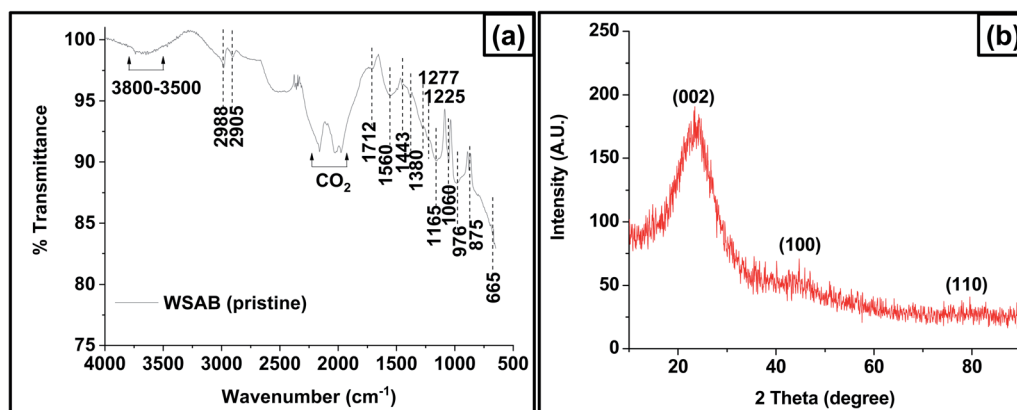


Fig. 2 (a) FTIR and (b) XRD spectra of walnut shell activated biochar.

Table 3 Pseudo-first order and pseudo-second order kinetic parameters for ibuprofen sorption at 25 °C at different WSAB doses and initial ibuprofen concentrations

Experimental $q_e$ (mg g <sup>-1</sup> )	Pseudo-first order			Pseudo-second order			
	$q_e$ (mg g <sup>-1</sup> )	$k_1$ (h <sup>-1</sup> )	$R^2$	$q_e$ (mg g <sup>-1</sup> )	$k_2$ (g mg <sup>-1</sup> h <sup>-1</sup> )	$R^2$	
<b>At different WSAB doses (g L<sup>-1</sup>)</b>							
0.5	75.83	20.17	0.07	0.782	76.34	0.01	0.998
1.0	42.98	8.19	0.06	0.560	43.48	0.03	0.999
2.0	24.25	3.1	0.03	0.447	24.21	0.08	0.999
<b>At different initial ibuprofen concentrations (mg L<sup>-1</sup>)</b>							
25	24.46	4.10	0.006	0.389	24.33	0.05	0.995
50	42.98	8.19	0.01	0.560	43.48	0.03	0.999
110	69.64	15.00	0.01	0.776	70.92	0.02	0.997



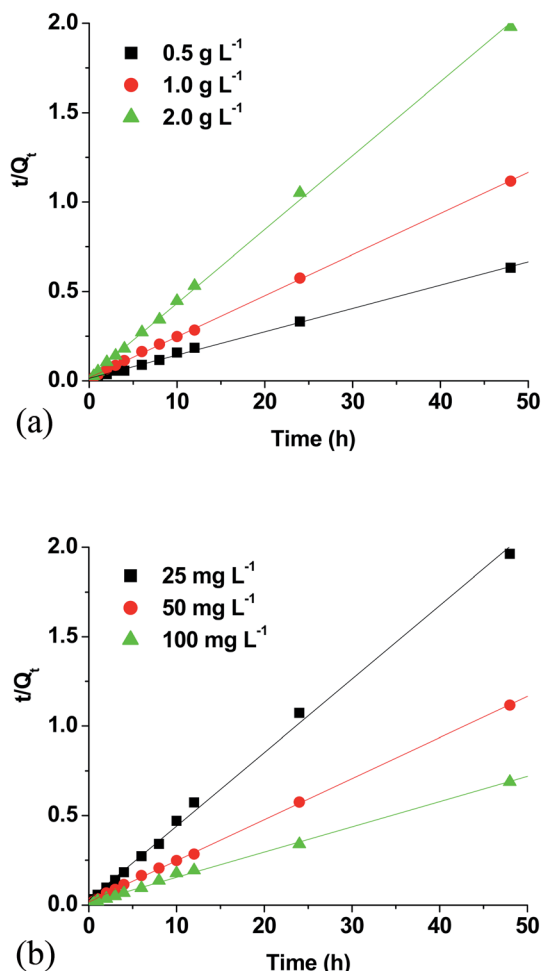


Fig. 3 Pseudo-second order kinetic plots (a) dose kinetics at 0.5, 1.0 and 2.0 g L<sup>-1</sup> WSAB; (b) ibuprofen conc. kinetics at 25, 50, and 100 mg L<sup>-1</sup> [temp. 25 °C, pH 4.0].

and Langmuir isotherm equations (Fig. 4). Maximum Langmuir capacities were 69.73, 68.05 and 66.98 mg g<sup>-1</sup> at 25, 35 and 45 °C, respectively (Table 4). The maximum adsorption capacities remained almost constant with temperature (Table 4). Both models have high correlation coefficient ( $R^2$ ) values (Table 4), which suggests that monolayer and multilayer sorptions occur simultaneously. This also supports diverse sorption processes

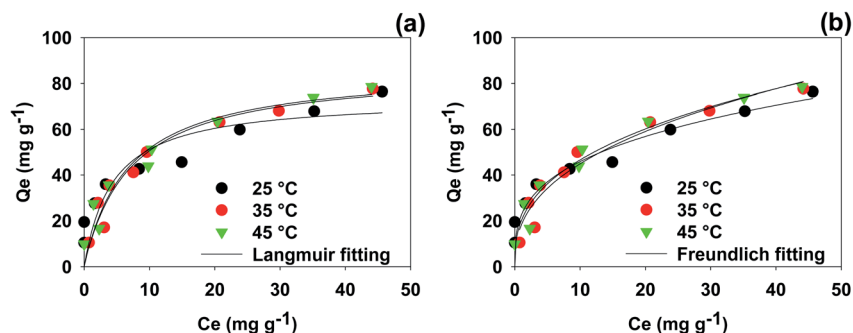


Fig. 4 Ibuprofen isotherm plots at 25, 35, and 45 °C; (a) Langmuir and (b) Freundlich [initial pH 4.0, WSAB dose 1.0 g L<sup>-1</sup>].

Table 4 Langmuir and Freundlich isotherm constants for ibuprofen sorption on WSAB at 25, 35, and 45 °C

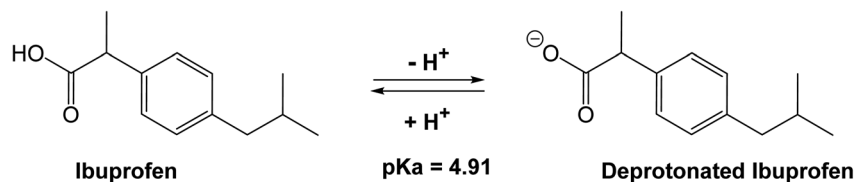
Isotherms	Parameters	Temperature (°C)		
		25	35	45
Freundlich	$K_F$ (mg g <sup>-1</sup> )	22.5	20.0	18.1
	$1/n$	0.31	0.37	0.40
	$n$	3.23	2.72	2.53
	$R^2$	0.86	0.94	0.94
	SEE	8.85	6.24	5.91
Langmuir	$Q^\circ$ (mg g <sup>-1</sup> )	69.7	68.1	67.0
	$b$ (L mg <sup>-1</sup> )	0.29	0.15	0.14
	$R^2$	0.79	0.92	0.95
	SEE	10.84	7.26	5.36

(Schemes 2–6) proceeding simultaneously. Walnut shell activated biochar's sorption efficiency ( $\sim 70$  mg g<sup>-1</sup> at 25 °C) is higher than those of most biochars and modified biochars reported in the literature (Table 5).

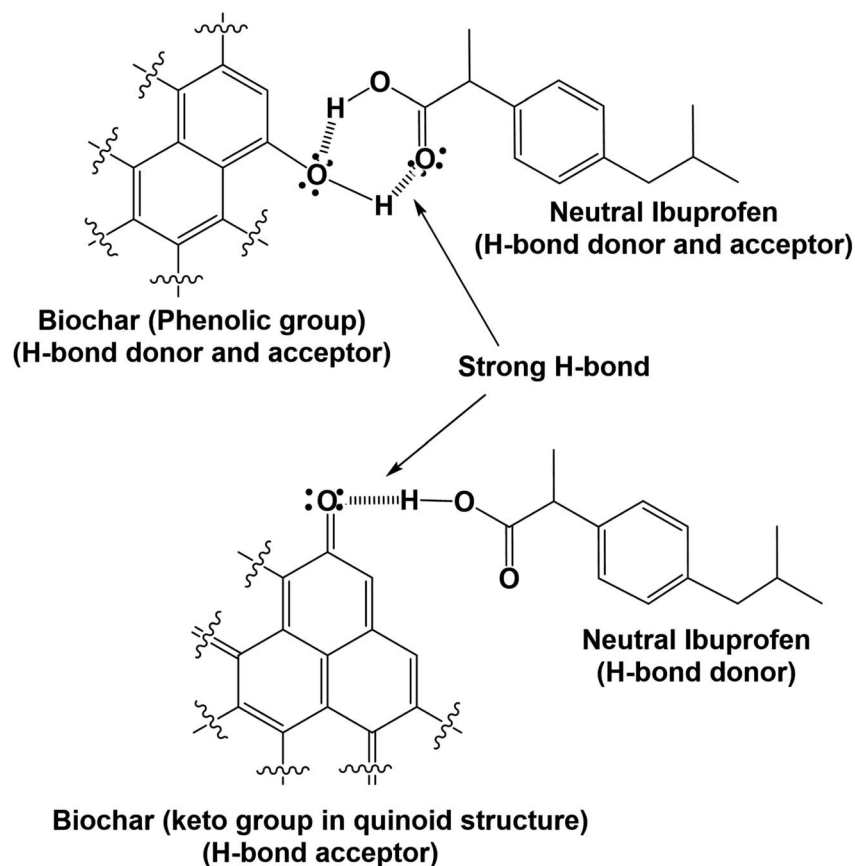
**3.2.3. Effect of the initial solution pH.** The initial solution pH played a very significant role in ibuprofen adsorption (Fig. 5) both by influencing the surface properties of WSAB and by altering ibuprofen's speciation. Ibuprofen adsorption is higher in acidic pH with the maximum adsorption at pH 4. Lowering pH below 4 or increasing pH above 4 causes ibuprofen uptake to fall (Fig. 5). The decrease in ibuprofen sorption with a drop in pH from 4.0 to 2.0 is due to the presence of only the neutral form of ibuprofen, and at pH 2, the net surface charge on WSAB drops to zero ( $pH_{zpc}$  of WSAB = 2.0). As the pH increases from 2.0 to above 4.0, the WSAB surface becomes net negatively charged, and ibuprofen is increasingly ionized to its carboxylate form. This decreases sorption by electrostatic repulsion (Fig. 5, Scheme 5). Similar trends for ibuprofen adsorption were also reported in several studies.<sup>5,11,13–17,56</sup>

**3.2.4. Ibuprofen adsorption mechanism onto WSAB.** Ibuprofen ( $pK_a = 4.9$ ) contains one aliphatic carboxylic group ( $-COOH$ ) which can deprotonate to ( $-COO^-$ ). Scheme 1 shows the deprotonated and neutral forms of ibuprofen. Ibuprofen is predominately deprotonated at  $pH > 4.9$  ( $pH > pK_a$ ), while it exists mostly as neutral at  $pH < pK_a$ . At pH 4.0, the activated biochar surface has a net negative charge ( $pH > pH_{zpc}$ ), but ibuprofen will be mostly neutral ( $COOH$ ). This neutral form will

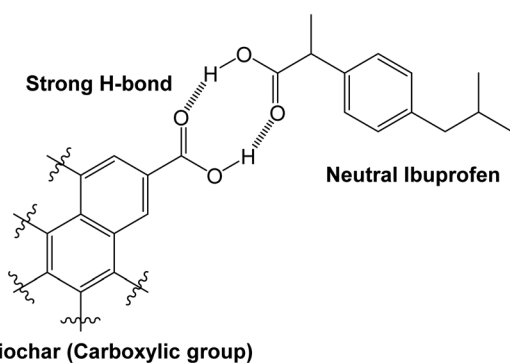




Scheme 1 Ibuprofen protonation-deprotonation showing both neutral and deprotonated forms.



Scheme 2 Proposed hydrogen bonding between neutral ibuprofen and WSAB's phenolic groups.

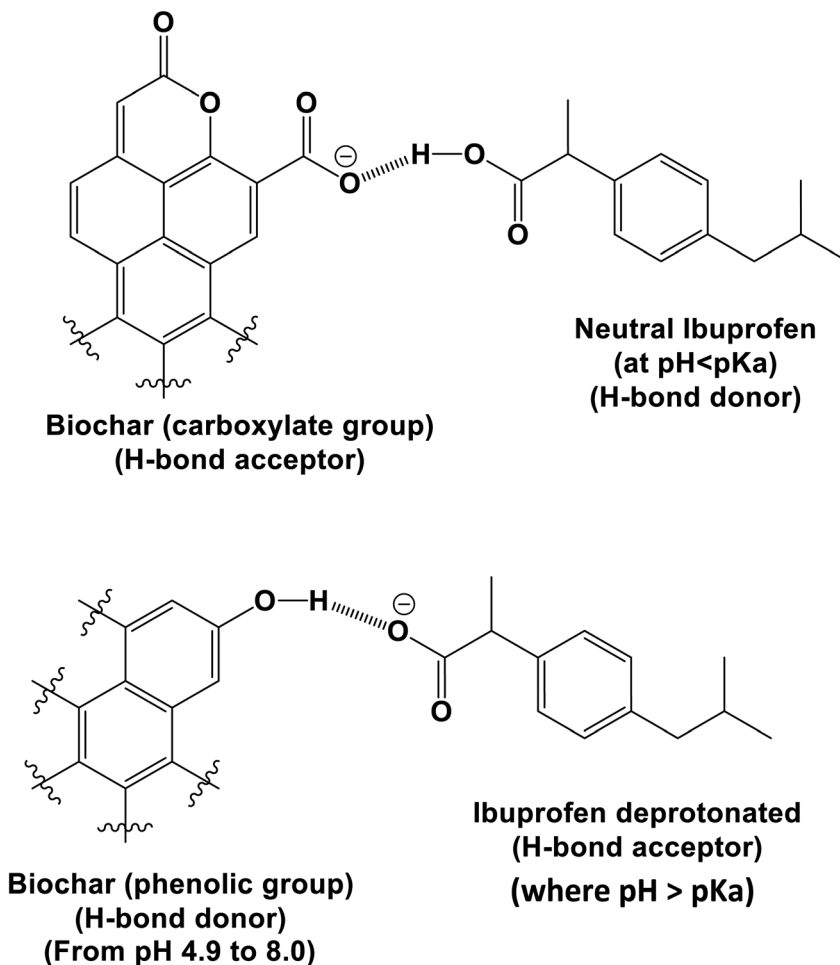


Scheme 3 Hydrogen bonding between neutral ibuprofen and carboxylic functional groups of WSAB.

H-bond strongly with deprotonated surface oxygen sites on the WSBC net negative surface. However, at  $\text{pH} > 4.9$  ( $\text{pH} > \text{pK}_a$ ), ibuprofen is largely in its carboxylate form, resulting in the drop in ibuprofen adsorption on WSAB due to electrostatic repulsion ( $\text{pH}_{\text{zpc}} \sim 2.0$ ). The carboxylate form experiences repulsion from the negatively charged WSAB surface. Electrostatic attraction plays a minor role in adsorption because ibuprofen never becomes protonated (positively charged) at a pH where the WSAB surface becomes negatively charged ( $\text{pH} > 2$ ). H-bonding, van der Waals forces and pore diffusion serve as sorption attractions.<sup>2,17</sup> Ibuprofen's aromatic ring might also engage in  $\pi$ - $\pi$  donor-acceptor stacking with electron deficient aromatic sites on the WSAB. The two *p*-aliphatic substituents on this ring have branched structures which might sterically hinder such interactions, but they also enrich the  $\pi$ -electron density on the ring favoring the  $\pi$ -stacking shown on the upper left of Scheme







Scheme 4 WSBC hydrogen bonding from ibuprofen (pH < pK<sub>a</sub>) and to ibuprofen (pH > pK<sub>a</sub>).

6. Ibuprofen's water solubility increases as pH increases, and it becomes completely ionized to its carboxylate form. This will alter the change in free energy experienced going from the solution to the adsorbed state in complex ways that involve both the  $\Delta H$  and  $T\Delta S$  terms of  $\Delta G$ . The hydrophobicity of the carboxylate form is much less than that of the neutral carboxylic form. Contribution to favoring the sorption *versus* the solution state of both ibuprofen forms is a very complex topic. The Gibbs free energy was negative ( $-28.4$ ,  $-27.7$  and  $-28.4$  kJ mol<sup>-1</sup>) for sorption at 25, 35 and 45 °C, respectively. Ibuprofen sorption was spontaneous on WSAB, and sorption remains almost constant with temperature changes. Possible ibuprofen/WSAB interactions are shown in Schemes 2–6. H-bonding contributors are more easily discussed, but other major contributors and the role of entropy ( $\Delta S$ ) are really impossible to clarify in molecular terms.

WSAB contains oxygen-containing surface functional groups such as carboxyls, quinones, lactones and phenols that play important roles in adsorption.<sup>2,57</sup> The elemental analysis, FTIR and EDX data confirmed that these oxygen functional groups exist on the WSAB surface. These functional groups allow walnut shell activated biochar to act both as an H-bond donor and acceptor. These groups can form H-bonds with ibuprofen

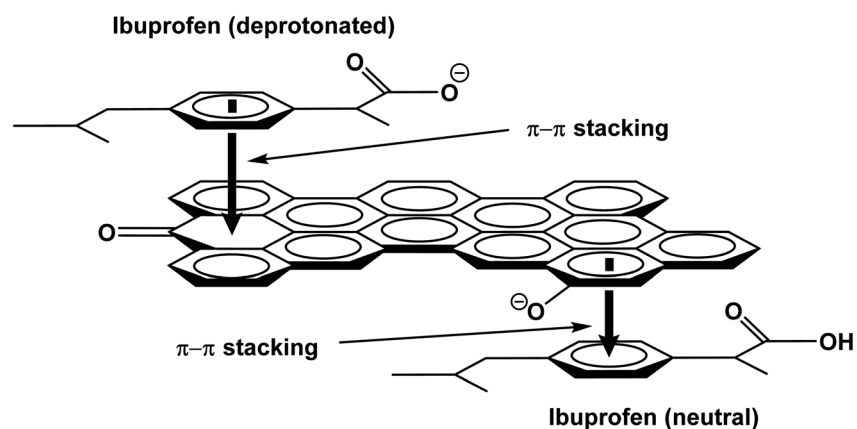
under various conditions as shown in Schemes 2–4. At pH 4.0, the point of maximum adsorption, ibuprofen is mostly in the neutral state. Its main H-bonding interactions are with phenolic, lactonic, carboxylic and ether groups (Schemes 2–4). Here, ibuprofen's -COOH group acts as a strong H-bond donor and as an H-bond acceptor. Chelation of ibuprofen with activated biochar may also happen in a similar fashion (Scheme 3).

At pH > 4.91, ibuprofen sorption is reduced. Ibuprofen is present in both its neutral and carboxylate forms. WSAB is now net negatively charged, resulting in more electrostatic repulsions (Scheme 5), lowering adsorption as pH increases. Pore diffusion and  $\pi$ - $\pi$ -interactions also enhance ibuprofen sorption on WSAB.<sup>2,17,33,48,58</sup> Ibuprofen's aromatic ring could interact with electron rich or electron deficient aromatic WSAB sites *via*  $\pi$ - $\pi$  electron-donor attractions. Phenolic hydroxyl groups increase aromatic ring electron density (and even more so upon their deprotonation to phenolate sites). This favors  $\pi$ - $\pi$  electron donation to neutral ibuprofen (Scheme 6). Such  $\pi$ - $\pi$  electron donation to neutral ibuprofen by carbonaceous adsorbents was previously invoked as a possible sorption interaction.<sup>2,16,17,44</sup> WSAB's large surface area (686 m<sup>2</sup> g<sup>-1</sup>) and porosity promote ibuprofen sorption through pore diffusion.





**Scheme 5** At high pH ( $\text{pH} > \text{both } \text{pH}_{\text{zpc}} \text{ and } \text{pK}_a$ ), both ibuprofen and WSAB are negatively charged, leading to charge–charge repulsions, thus decreasing the overall adsorption.



**Scheme 6**  $\pi$ - $\pi$  electron donor–acceptor attractions between neutral and deprotonated ibuprofen with aromatic rings on the WSAB surface.

**3.2.5. Column studies.** Fixed-bed column studies were performed to optimize the sorption process for use in future large-scale applications. Fixed-bed ibuprofen sorption was

performed, and the column parameters ( $C_b$ ,  $C_x$ ,  $t_b$ ,  $t_f$ ,  $t_x$ ,  $t_d$ ,  $V_b$ ,  $V_x$ ,  $\delta$ ,  $f$ , column capacity, breakthrough capacity, and percent saturation) were obtained (Table 6) from ibuprofen's fixed-bed





Table 5 Comparison of walnut activated biochar's (WSAB) ibuprofen adsorption Langmuir capacity with different biochars, modified biochars and other adsorbents reported in the literature

Precursor	Water type	pH	Conc. range (mg L <sup>-1</sup> )	Temp. (°C)	Surface area (m <sup>2</sup> g <sup>-1</sup> )	Adsorption capacity Q <sub>e</sub> (mg g <sup>-1</sup> )	Ref.
Walnut shell activated biochar (WSAB)	Aqueous solution	4	10–120	25	686	69.7	This study
				35		68.0	
				45		67.0	
Sugarcane bagasse physically activated biochar	Deionized water	2	1–50	20	—	11.9	44
Sugarcane bagasse chemically activated biochar	Deionized water			15	—	13.5	
Commercial biochar (W-biochar)	Deionized water	8.5	1–8	23	369.1	21.7	60
	Reclaimed reverse osmosis concentrate		2–11			12.5	
Pine wood fast pyrolysis biochar	Distilled water	3	25–100	35	1.35	10.7	17
Steam activated mung bean husk biochar	Deionized water	2	1–100	20	—	62.5	61
				25		62.5	
				30		55.5	
				35		55.5	
				40		43.7	
Chemically modified <i>Parthenium hysterophorus</i> derived biochar	Distilled water	2	5–100	20	308	3.8	62
				25		3.7	
				30		3.3	
				35		3.1	
Wood apple shell biochar	Distilled water	2.5	3–45	20	4.4	5.0	43
Wood apple shell steam activated biochar	Distilled water				308	12.7	
Steam activated date seed biochar	Deionized water	3	5–50	20	513	13.2	63
Chemically activated date seed biochar		3	5–50	20	342	11.2	
Physically activated <i>Cocos nucifera</i> shell biochar	Distilled water	2	1–50	20	726	9.4	64
Physically activated <i>Cocos nucifera</i> shell biochar		2	1–50	20	805	11.4	
Chilli seed biochar (C450)	Water	7	50–1000	25	0.52	12.8	65
Chilli seed biochar (C550)	Water	7	50–1000	25	0.24	16.7	
Chilli seed biochar (C600)	Water	7	50–1000	25	0.18	26.1	
Chilli seed biochar (C600)	Water	9	50–1000	25	0.18	19.8	
Chilli seed biochar (C600)	Water	11	50–1000	25	0.18	18.2	
Chilli seed biochar (C600)	Water	7	50–1000	15	0.18	24.7	
Chilli seed biochar (C600)	Water	7	50–1000	35	0.18	25.69	
Cross-linked magnetic chitosan/activated biochar	—	6	2.5	25	502	21.5	66
Chitosan-modified waste tire crumb rubber	Environmental water samples	—	—	25	—	17.7	67
Functionalized nano-clay composite	—	6	—	25	—	0.86	68

Table 5 (Contd.)

Precursor	Water type	pH	Conc. range (mg L <sup>-1</sup> )	Temp. (°C)	Surface area (m <sup>2</sup> g <sup>-1</sup> )	Adsorption capacity $Q_e$ (mg g <sup>-1</sup> )	Ref.
Autoclaved aerated concrete blocks (AAC)	Deionized water	—	0.1–10	—	—	1.54	69
Brickbats (BB)						0.94	
Blast furnace slag (BFS)						1.26	
Lightweight expanded clay aggregate (LECA)						1.59	
Natural pyrite (NP)	Wastewater	3	40	—	2.19	70	
Wood charcoal (WC)					736.5		
Natural zeolite (NZ)					429.8		
Raw CS-PVA					224.5		
Raw GO	Aqueous solution	7	1–10	25	356.9	71	
Raw AC					138.6		
AC/CS-PVA:3.0					160.8		
GO/CS-PVA:3.0					146.3		
Genipin-crosslinked chitosan/graphene oxide-SO <sub>3</sub> H				35			
				45			

sorption graph (Fig. 6). Section 2.6 provides the background on these terms, and Table 6 also defines these parameters. The increase in the effluent ibuprofen concentration is less steep, indicating the less efficient utilization of the biochar fixed-bed. Thus, only an 89% column saturation at the exhaustion point is achieved (Table 6). The column capacity was 30.08 mg g<sup>-1</sup>, and the breakpoint capacity was 15.6 mg g<sup>-1</sup>. Low column capacity might be due to the presence of a wide mass transfer zone.<sup>34</sup> The column almost cleaned 5 L of ibuprofen contaminated water before reaching to the breakthrough point (Fig. 6). The slower saturation and delay in breakthrough are due to the larger surface area of the WSAB, which increased the number of surface active sites for excellent ibuprofen sorption.<sup>39</sup> The breakthrough point occurs when the effluent's adsorbate concentration started increasing due to a decrease in the mass transfer zone. An adsorbent with excellent sorption capacity (WSAB with a maximum Langmuir capacity of ~70 mg g<sup>-1</sup>) gave a delay in the time to breakthrough due to complete ibuprofen sorption during the initial phase. Low column capacity (30.08 mg g<sup>-1</sup>) versus batch capacity (~70 mg g<sup>-1</sup>) for WSAB was obtained. The empty bed's contact time with the contaminated water of 21.2 min is much shorter (~70 times shorter) than the batch equilibrium time of 24 h. Thus, the column takes a long time to reach equilibrium and breakthrough.

The experimental column data were also fitted to the Adams-Bohart and Thomas models described in section 2. The Adams-Bohart and Thomas fitting figures are provided in S6 and S7,† respectively. The data obtained from Adams-Bohart and Thomas model fitting are provided in Table 6. Both models showed high correlations ( $R^2 = 0.88$ ) with the sorption data. The column saturation concentration ( $N_0$ ) obtained through the Adams-Bohart model is 29.5 mg L<sup>-1</sup>. Equilibrium ibuprofen uptake per gram WSAB ( $q_0$ ) obtained by the Thomas model is 35.9 mg g<sup>-1</sup>. This is reasonably close to an experimental column capacity of 30.08 mg g<sup>-1</sup>, supporting the applicability of the Thomas model to column data.

Usually, the pharmaceutical concentrations in natural systems are in the ng L<sup>-1</sup> to µg L<sup>-1</sup> range.<sup>2</sup> However, in industrial effluents, concentrations are in µg L<sup>-1</sup> and occasionally increases to the 1 mg L<sup>-1</sup> range.<sup>2</sup> Assuming a maximum 1 mg L<sup>-1</sup> environmentally relevant concentration, one-gram WSAB can treat approximately 30 L ibuprofen contaminated water under ideal column conditions. This shows high applicability for WSAB. Sorption decontamination would most likely be applied to point emissions to the environment such as factories, hospitals and similar effluents or specific streams in wastewater treatment plants. Studies of low ibuprofen concentrations were not yet performed.

### 3.3. Cost estimation

The preparation cost of walnut shell activated biochar (WSAB) can be estimated using equations provided in section 2.6.

$$\text{COST}_{\text{BC}} = (\text{COST}_{\text{P}} + \text{COST}_{\text{Pro}} + \text{COST}_{\text{A/M}} + \text{COST}_{\text{C}}) + \text{OTHER COSTS}$$



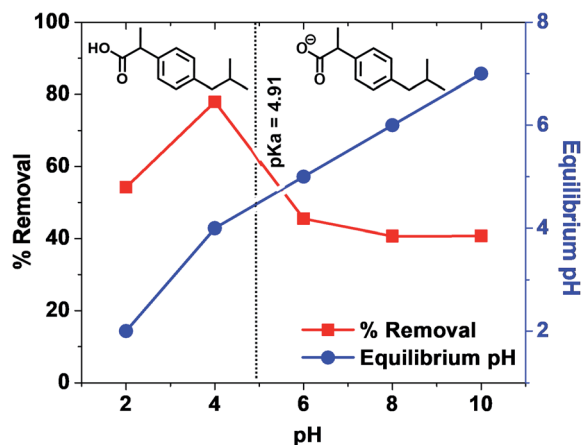


Fig. 5 Effect of the initial pH on ibuprofen sorption using WSAB [temperature 25 °C, initial ibuprofen concentration 50 mg L<sup>-1</sup>, and WSAB dose 1.0 g L<sup>-1</sup>].

$$\text{COST}_{\text{BC}} = \text{US\$ } 0.44 + \text{US\$ } 1.26 + \text{US\$ } 3.14 + \text{US\$ } 1.46 + \text{US\$ } 0.63 = \text{US\$ } 6.39 \text{ kg}^{-1}$$

- $\text{COST}_{\text{P}} = \text{Precursor cost} + \text{transportation cost} + \text{packing and storage cost} = \text{US\$ } 0.44 \text{ kg}^{-1}$
- Precursor cost [precursor procurement] = US\$ 0.19 kg<sup>-1</sup>

Table 6 Fixed-bed column parameters obtained for ibuprofen sorption on WSAB

Parameters	Results
Weight of WSAB	2.0 g
Bed depth	3.5 cm
Bed volume	11.0 cm <sup>3</sup>
Flow rate	2.1 mL min <sup>-1</sup>
EBCT (empty-bed-contact-time)	21.2 min
Biochar usage rate	0.0004 g L <sup>-1</sup>
Column capacity	30.1 mg g <sup>-1</sup>
Breakpoint capacity	15.6 mg g <sup>-1</sup>
Initial concentration (C <sub>0</sub> )	0.0075 mg mL <sup>-1</sup>
Ibuprofen concentration at the exhaustion point (C <sub>x</sub> )	0.005 mg mL <sup>-1</sup>
Ibuprofen concentration at the break point (C <sub>b</sub> )	ND
Exhaustion volume (V <sub>x</sub> )	48.5 mg cm <sup>-2</sup>
Break point volume (V <sub>b</sub> )	15.9 mg cm <sup>-2</sup>
Total time to reach the exhaustion point (t <sub>x</sub> )	7340 minutes
Total time to reach the break point (t <sub>b</sub> )	1878 minutes
Percent saturation	99.8
Primary adsorption zone length (δ), cm	2.60
Fractional capacity (f)	0.88
<b>Adams-Bohart model</b>	
K <sub>AB</sub> (g min L <sup>-1</sup> )	0.067
N <sub>0</sub> (g L <sup>-1</sup> )	29.53
R <sup>2</sup>	0.88
<b>Thomas model</b>	
K <sub>TH</sub> (g min L <sup>-1</sup> )	0.067
q <sub>0</sub> (g g <sup>-1</sup> )	35.93
R <sup>2</sup>	0.88

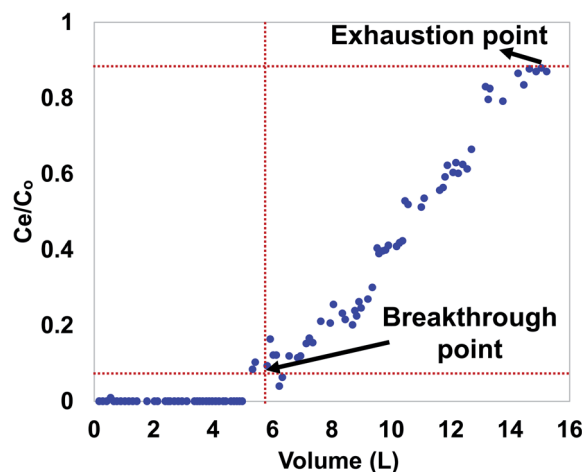


Fig. 6 Ibuprofen uptake on WSAB fixed-bed column. A graph showing the breakpoint and saturation at the exhaustion point (initial ibuprofen concentration 7.5 mg L<sup>-1</sup>, pH 4.0, and column bed length ~4 cm; hydraulic flow rate of 2.5 mL min<sup>-1</sup>; WSAB dose 2.0 g).

- Transportation cost + packaging/storage etc. = US\$ 0.23 + 2 = US\$ 0.025 kg<sup>-1</sup> = US\$ 0.255 kg<sup>-1</sup> (this cost will be reduced for large scale precursor procurement)  $\text{COST}_{\text{Pro}} = (\text{cleaning cost} + \text{drying cost} + \text{labor cost for precursor size reduction}) = (\text{US\$ } 0.19 + \text{US\$ } 0.20 + \text{US\$ } 0.87) = \text{US\$ } 1.26 \text{ kg}^{-1}$

- (Cleaning cost = precursor cleaning using tap water followed by distilled water = US\$ 0.19 kg<sup>-1</sup>)

- Drying cost = sun drying + oven drying (sun drying = US\$ 0.0 kg<sup>-1</sup>) + (oven drying for 2 h for ensuring complete drying of the precursor = 2 × 1 KW = 2 KW = 2 × 8 (tariff rate) = US\$ 0.20 kg<sup>-1</sup>), (note: this cost will be less for large scale operations) = total = US\$ 0.20 kg<sup>-1</sup>

- Labor cost for precursor sizing = US\$ 0.87 (unskilled labor cost ~@ US\$ 6.91/8 h) (this cost will be reduced for large scale operations involving grinding/sizing machines)

- $\text{COST}_{\text{A/M}} = \text{activation cost (procurement of } o\text{-phosphoric acid used for biochar activation)} = \text{US\$ } 3.14 \text{ kg}^{-1}$

- $\text{COST}_{\text{C}} = (\text{pyrolysis} + \text{nitrogen gas cost}) = \text{US\$ } 1.49 \text{ kg}^{-1}$
- (Total furnace running time × power consumption per hour × tariff rate) = (2 h × 4.4 KW × 8) = US\$ 0.88 kg<sup>-1</sup>

- (Nitrogen usage = total flow × cost) = US\$ 0.23 kg<sup>-1</sup>

Total gas flow = 0.1 m<sup>3</sup> per hour × 3 = 0.3 m<sup>3</sup>

Cost = US\$ 0.075 per m<sup>3</sup>

Biochar washing = US\$ 0.35 kg<sup>-1</sup> (distilled water was used; its approximate cost is based on the electricity usage and water tariffs)

- **OTHER COSTS** = 10% offset (including wastewater recycling and waste disposal) = US\$ 0.63 kg<sup>-1</sup>

Biochars can be inexpensive or have negligible cost due to less expensive production techniques and waste utilization for biochar preparation.<sup>46</sup> In this study, walnut shells were obtained from a local market free of cost, but US\$ 0.18 kg<sup>-1</sup> was included based on the market cost. The total preparation cost of WSAB is estimated to be US\$ 6.93 kg<sup>-1</sup>. This cost can further be reduced by scaling up the biochar production for commercial purpose. The approximate cost of WSAB (US\$ 6.93 kg<sup>-1</sup>) is



comparable or lower than those of chitosan (US\$ 16 kg<sup>-1</sup>), chitosan based adsorbents (US\$ 8–10 kg<sup>-1</sup>), commercial activated carbons (US\$ 20–22 kg<sup>-1</sup>), and ion exchange resins (US\$ 150 kg<sup>-1</sup>) used for the pharmaceutical removal.<sup>47</sup>

## 4. Conclusions

Waste walnut shells were successfully used to prepare walnut shell-activated biochar (WSAB). This activated biochar was characterized and successfully applied for aqueous ibuprofen removal. The maximum ibuprofen sorption was achieved at pH 4.0. An excellent Langmuir adsorption capacity of 69.7 mg g<sup>-1</sup> was achieved; highlighting WSAB's potential for removing ibuprofen. This may extend to many organic pollutants and emerging pharmaceuticals. WSAB has a higher ibuprofen sorption than most biochars reported in the literature. Column studies gave a promising sorption capacity of 30.1 mg g<sup>-1</sup>. This work mandates a broad general study of WSAB for adsorption of pharmaceuticals and organic contaminants in general. Sorption interactions include H-bonding, hydrophobic interactions, van der Waals forces,  $\pi$ - $\pi$  attractions and pore diffusion for ibuprofen adsorption. The approximate production cost of US\$ 6.93 kg<sup>-1</sup> indicates WSAB as a low-cost adsorbent. Together with its easy availability and high sorption efficiency, WSAB is a sustainable sorbent for remediating ibuprofen from contaminated water.

## Conflicts of interest

No conflict of interest exists. We wish to confirm that there are no known conflicts of interest associated with this publication, and there has been no significant financial support for this work that could have influenced its outcome.

## Acknowledgements

The authors (DM and MP) are thankful to the Office of the Principal Scientific Adviser (PSA), Government of India (GOI) for financial assistance under the project “Delhi Cluster-Delhi Research Implementation and Innovation (DRIIV)”. Financial support [DST/TM/WTI/2K15/121 (C) dated: 19.09.2016] for the project entitled “Removal and Recovery of Pharmaceuticals from water using sustainable magnetic and nonmagnetic biochars” from the Department of Science and Technology, New Delhi, India, is also thankfully acknowledged.

## References

- 1 T. aus der Beek, F. A. Weber, A. Bergmann, S. Hickmann, I. Ebert, A. Hein and A. Küster, Pharmaceuticals in the environment—Global occurrences and perspectives, *Environ. Toxicol. Chem.*, 2016, **35**, 823–835.
- 2 M. Patel, R. Kumar, K. Kishor, T. Mlsna, C. U. Pittman Jr and D. Mohan, Pharmaceuticals of emerging concern in aquatic systems: chemistry, occurrence, effects, and removal methods, *Chem. Rev.*, 2019, **119**, 3510–3673.
- 3 S. R. Hughes, P. Kay and L. E. Brown, Global synthesis and critical evaluation of pharmaceutical data sets collected from river systems, *Environ. Sci. Technol.*, 2013, **47**, 661–677.
- 4 K. Kümmerer, The presence of pharmaceuticals in the environment due to human use—present knowledge and future challenges, *J. Environ. Manage.*, 2009, **90**, 2354–2366.
- 5 K. P. Singh, A. K. Singh, U. V. Singh and P. Verma, Optimizing removal of ibuprofen from water by magnetic nanocomposite using Box–Behnken design, *Environ. Sci. Pollut. Res.*, 2012, **19**, 724–738.
- 6 J. Fick, H. Söderström, R. H. Lindberg, C. Phan, M. Tysklind and D. J. Larsson, Contamination of surface, ground, and drinking water from pharmaceutical production, *Environ. Toxicol. Chem.*, 2009, **28**, 2522–2527.
- 7 D. J. Larsson, C. de Pedro and N. Paxeus, Effluent from drug manufactures contains extremely high levels of pharmaceuticals, *J. Hazard. Mater.*, 2007, **148**, 751–755.
- 8 D. Mohan, C. U. Pittman Jr and T. Mlsna, *Sustainable Biochar for Water and Wastewater Treatment*, Elsevier, 2022.
- 9 M. Patel, A. K. Chaubey, C. M. Navarathna, T. Mlsna, C. U. Pittman Jr and D. Mohan, in *Sustainable Biochar for Water and Wastewater Treatment*, ed. D. Mohan, C. U. Pittman Jr and T. Mlsna, 2022, ch. 11, pp. 395–427.
- 10 J. Rivera-Utrilla, M. Sánchez-Polo, M. Á. Ferro-García, G. Prados-Joya and R. Ocampo-Pérez, Pharmaceuticals as emerging contaminants and their removal from water. A review, *Chemosphere*, 2013, **93**, 1268–1287.
- 11 A. S. Mestre, J. Pires, J. M. Nogueira and A. P. Carvalho, Activated carbons for the adsorption of ibuprofen, *Carbon*, 2007, **45**, 1979–1988.
- 12 N. H. Tran, M. Reinhard and K. Y.-H. Gin, Occurrence and fate of emerging contaminants in municipal wastewater treatment plants from different geographical regions-A review, *Water Res.*, 2018, **133**, 182–207.
- 13 T. X. Bui and H. Choi, Adsorptive removal of selected pharmaceuticals by mesoporous silica SBA-15, *J. Hazard. Mater.*, 2009, **168**, 602–608.
- 14 A. S. Mestre, A. S. Bexiga, M. Proença, M. Andrade, M. L. Pinto, I. Matos, I. M. Fonseca and A. P. Carvalho, Activated carbons from sisal waste by chemical activation with K<sub>2</sub>CO<sub>3</sub>: kinetics of paracetamol and ibuprofen removal from aqueous solution, *Bioresour. Technol.*, 2011, **102**, 8253–8260.
- 15 A. S. Mestre, J. Pires, J. M. Nogueira, J. B. Parra, A. P. Carvalho and C. O. Ania, Waste-derived activated carbons for removal of ibuprofen from solution: role of surface chemistry and pore structure, *Bioresour. Technol.*, 2009, **100**, 1720–1726.
- 16 S. P. Dubey, A. D. Dwivedi, M. Sillanpää and K. Gopal, Artemisia vulgaris-derived mesoporous honeycomb-shaped activated carbon for ibuprofen adsorption, *Chem. Eng. J.*, 2010, **165**, 537–544.
- 17 M. Essandoh, B. Kunwar, C. U. Pittman Jr, D. Mohan and T. Mlsna, Sorptive removal of salicylic acid and ibuprofen from aqueous solutions using pine wood fast pyrolysis biochar, *Chem. Eng. J.*, 2015, **265**, 219–227.



- 18 S. Gupta, G. K. Gupta and M. K. Mondal, Slow pyrolysis of chemically treated walnut shell for valuable products: Effect of process parameters and in-depth product analysis, *Energy*, 2019, **181**, 665e676.
- 19 APEDA, [https://agriexchange.apeda.gov.in/India%20Production/India\\_Productions.aspx?cat=fruit&hcode=1061](https://agriexchange.apeda.gov.in/India%20Production/India_Productions.aspx?cat=fruit&hcode=1061), 2021.
- 20 T.-H. Wang, M.-H. Li and S.-P. Teng, Bridging the gap between batch and column experiments: A case study of Cs adsorption on granite, *J. Hazard. Mater.*, 2009, **161**, 409–415.
- 21 A. G. Karunanayake, C. M. Navarathna, S. R. Gunatilake, M. Crowley, R. Anderson, D. Mohan, F. Perez, C. U. Pittman Jr and T. Mlsna, Fe<sub>3</sub>O<sub>4</sub> nanoparticles dispersed on Douglas fir biochar for phosphate sorption, *ACS Appl. Nano Mater.*, 2019, **2**, 3467–3479.
- 22 D. Mohan, A. Sarswat, V. K. Singh, M. Alexandre-Franco and C. U. Pittman Jr, Development of magnetic activated carbon from almond shells for trinitrophenol removal from water, *Chem. Eng. J.*, 2011, **172**, 1111–1125.
- 23 ASTM, *Standard Method for Chemical Analysis of Wood Charcoal*, American Society for Testing and Materials international, West Conshohocken, PA, USA, 2007.
- 24 S. C. Capareda, in *Sustainable Biochar for Water and Wastewater Treatment*, ed. D. Mohan, C. U. Pittman Jr and T. E. Mlsna, Elsevier, 2022, pp. 93–134, DOI: [10.1016/B978-0-12-822225-6.00013-0](https://doi.org/10.1016/B978-0-12-822225-6.00013-0).
- 25 S. Lagergren, About the theory of so-called adsorption of soluble substances, *K. Sven. Vetenskapsakad. Handl.*, 1898, **24**, 1–39.
- 26 Y.-S. Ho and G. McKay, Pseudo-second order model for sorption processes, *Process Biochem.*, 1999, **34**, 451–465.
- 27 H. M. F. Freundlich, Over the adsorption in solution, *J. Phys. Chem.*, 1906, **57**, 1100–1107.
- 28 I. Langmuir, The constitution and fundamental properties of solids and liquids. Part I. Solids, *J. Am. Chem. Soc.*, 1916, **38**, 2221–2295.
- 29 D. Mohan, A. K. Chaubey, M. Patel, C. Navarathna, T. Mlsna and C. U. Pittman Jr, in *Sustainable Biochar for Water and Wastewater Treatment*, ed. D. Mohan, C. U. Pittman Jr and T. Mlsna, Elsevier, 2022, ch. 5, pp. 153–203.
- 30 R. Sharma, A. Sarswat, C. U. Pittman Jr and D. Mohan, Cadmium and lead remediation using magnetic and non-magnetic sustainable biosorbents derived from Bauhinia purpurea pods, *RSC Adv.*, 2017, **7**, 8606–8624.
- 31 A. Sarswat and D. Mohan, Sustainable development of coconut shell activated carbon (CSAC) & a magnetic coconut shell activated carbon (MCSAC) for phenol (2-nitrophenol) removal, *RSC Adv.*, 2016, **6**, 85390–85410.
- 32 N. B. Dewage, R. E. Fowler, C. U. Pittman Jr, D. Mohan and T. Mlsna, Lead (Pb<sup>2+</sup>) sorptive removal using chitosan-modified biochar: batch and fixed-bed studies, *RSC Adv.*, 2018, **8**, 25368–25377.
- 33 V. Vimal, M. Patel and D. Mohan, Aqueous carbofuran removal using slow pyrolyzed sugarcane bagasse biochar: equilibrium and fixed-bed studies, *RSC Adv.*, 2019, **9**, 26338–26350.
- 34 V. Choudhary, M. Patel, C. U. Pittman Jr and D. Mohan, Batch and Continuous Fixed-Bed Lead Removal Using Himalayan Pine Needle Biochar: Isotherm and Kinetic Studies, *ACS Omega*, 2020, **5**, 16366–16378.
- 35 V. K. Gupta, S. K. Srivastava, D. Mohan and S. Sharma, Design parameters for fixed bed reactors of activated carbon developed from fertilizer waste for the removal of some heavy metal ions, *Waste Manag.*, 1998, **17**, 517–522.
- 36 T. W. Weber and R. K. Chakravorty, Pore and solid diffusion models for fixed-bed adsorbers, *AIChE J.*, 1974, **20**, 228–238.
- 37 H. Kumar, M. Patel and D. Mohan, Simplified Batch and Fixed-Bed Design System for Efficient and Sustainable Fluoride Removal from Water Using Slow Pyrolyzed Okra Stem and Black Gram Straw Biochars, *ACS Omega*, 2019, **4**(22), 19513–19525.
- 38 D. Mohan and S. Chander, Removal and recovery of metal ions from acid mine drainage using lignite—a low cost sorbent, *J. Hazard. Mater.*, 2006, **137**, 1545–1553.
- 39 C. Navarathna, P. M. Rodrigo, V. S. Thrikawala, A. Ramirez, T. E. Mlsna, C. U. Pittman Jr, and D. Mohan in *Sustainable Biochar for Water and Wastewater Treatment*, ed. D. Mohan, T. E. Mlsna and C. U. Pittman Jr, Elsevier, 2022, ch. 15, vol. 1, pp. 527–554.
- 40 G. Bohart and E. Adams, Some aspects of the behavior of charcoal with respect to chlorine, *J. Am. Chem. Soc.*, 1920, **42**, 523–544.
- 41 H. C. Thomas, Heterogeneous ion exchange in a flowing system, *J. Am. Chem. Soc.*, 1944, **66**, 1664–1666.
- 42 A. Ahmad and B. Hameed, Fixed-bed adsorption of reactive azo dye onto granular activated carbon prepared from waste, *J. Hazard. Mater.*, 2010, **175**, 298–303.
- 43 P. Chakraborty, S. Banerjee, S. Kumar, S. Sadhukhan and G. Halder, Elucidation of ibuprofen uptake capability of raw and steam activated biochar of Aegle marmelos shell: Isotherm, kinetics, thermodynamics and cost estimation, *Process Saf. Environ. Prot.*, 2018, **118**, 10–23.
- 44 P. Chakraborty, S. Show, S. Banerjee and G. Halder, Mechanistic insight into sorptive elimination of ibuprofen employing bi-directional activated biochar from sugarcane bagasse: Performance evaluation and cost estimation, *J. Environ. Chem. Eng.*, 2018, **6**, 5287–5300.
- 45 R. Kumar, M. Patel, P. Singh, J. Bundschuh, C. U. Pittman Jr, L. Trakal and D. Mohan, Emerging technologies for arsenic removal from drinking water in rural and peri-urban areas: Methods, experience from, and options for Latin America, *Sci. Total Environ.*, 2019, **694**, 133427.
- 46 M. B. Ahmed, J. L. Zhou, H. H. Ngo and W. Guo, Adsorptive removal of antibiotics from water and wastewater: progress and challenges, *Sci. Total Environ.*, 2015, **532**, 112–126.
- 47 J. I. R. de Andrade, M. F. Oliveira, M. G. da Silva and M. G. Vieira, Adsorption of pharmaceuticals from water and wastewater using nonconventional low-cost materials: a review, *Ind. Eng. Chem. Res.*, 2018, **57**, 3103–3127.
- 48 M. Patel, R. Kumar, C. U. Pittman Jr and D. Mohan, Ciprofloxacin and acetaminophen sorption onto banana peel biochars: Environmental and process parameter influences, *Environ. Res.*, 2021, **201**, 111218.



- 49 D. Mohan, K. Abhishek, A. Sarswat, M. Patel, P. Singh and C. U. Pittman Jr, Biochar production and applications in soil fertility and carbon sequestration—a sustainable solution to crop-residue burning in India, *RSC Adv.*, 2018, **8**, 508–520.
- 50 A. U. Rajapaksha, M. Vithanage, M. Zhang, M. Ahmad, D. Mohan, S. X. Chang and Y. S. Ok, Pyrolysis condition affected sulfamethazine sorption by tea waste biochars, *Bioresour. Technol.*, 2014, **166**, 303–308.
- 51 R. M. Silverstein, F. X. Webster, D. J. Kiemle and D. L. Bryce, in *Spectrometric Identification of Organic Compounds*, Wiley-VCH, 8th edn, 2014.
- 52 S. Mayakaduwa, M. Vithanage, A. Karunarathna, D. Mohan and Y. S. Ok, Interface interactions between insecticide carbofuran and tea waste biochars produced at different pyrolysis temperatures, *Chem. Speciat. Bioavailab.*, 2016, **28**, 110–118.
- 53 D. Qu, Studies of the activated carbons used in double-layer supercapacitors, *J. Power Sources*, 2002, **109**, 403–411.
- 54 A. Dandekar, R. Baker and M. Vannice, Characterization of activated carbon, graphitized carbon fibers and synthetic diamond powder using TPD and DRIFTS, *Carbon*, 1998, **36**, 1821–1831.
- 55 W. Tong, Q. Liu, S. Ren, J. Zhou, T. Zhang and C. Yang, Effect of pyrolysis temperature on pine sawdust chars and their gasification reactivity mechanism with CO<sub>2</sub>, *Asia-Pac. J. Chem. Eng.*, 2018, **13**, e2256.
- 56 R. Baccar, M. Sarrà, J. Bouzid, M. Feki and P. Blánquez, Removal of pharmaceutical compounds by activated carbon prepared from agricultural by-product, *Chem. Eng. J.*, 2012, **211**, 310–317.
- 57 H. Liu, W. Ning, P. Cheng, J. Zhang, Y. Wang and C. Zhang, Evaluation of animal hairs-based activated carbon for sorption of norfloxacin and acetaminophen by comparing with cattail fiber-based activated carbon, *J. Anal. Appl. Pyrolysis*, 2013, **101**, 156–165.
- 58 N. B. Dewage, A. S. Liyanage, Q. Smith, C. U. Pittman Jr, F. Perez, D. Mohan and T. Mlsna, Fast aniline and nitrobenzene remediation from water on magnetized and nonmagnetized Douglas fir biochar, *Chemosphere*, 2019, **225**, 943–953.
- 59 K. Wojtacha-Rychter and A. Smoliński, A study of dynamic adsorption of propylene and ethylene emitted from the process of coal self-heating, *Sci. Rep.*, 2019, **9**, 1–14.
- 60 L. Lin, W. Jiang and P. Xu, Comparative study on pharmaceuticals adsorption in reclaimed water desalination concentrate using biochar: Impact of salts and organic matter, *Sci. Total Environ.*, 2017, **601**, 857–864.
- 61 S. Mondal, K. Bobde, K. Aikat and G. Halder, Biosorptive uptake of ibuprofen by steam activated biochar derived from mung bean husk: Equilibrium, kinetics, thermodynamics, modeling and eco-toxicological studies, *J. Environ. Manage.*, 2016, **182**, 581–594.
- 62 S. Mondal, K. Aikat and G. Halder, Biosorptive uptake of ibuprofen by chemically modified Parthenium hysterophorus derived biochar: Equilibrium, kinetics, thermodynamics and modeling, *Ecol. Eng.*, 2016, **92**, 158–172.
- 63 P. Chakraborty, S. D. Singh, I. Gorai, D. Singh, W.-U. Rahman and G. Halder, Explication of physically and chemically treated date stone biochar for sorptive removal of ibuprofen from aqueous solution, *J. Water Proc. Eng.*, 2020, **33**, 101022.
- 64 P. Chakraborty, S. Show, W. U. Rahman and G. Halder, Linearity and non-linearity analysis of isotherms and kinetics for ibuprofen removal using superheated steam and acid modified biochar, *Process Saf. Environ. Prot.*, 2019, **126**, 193–204.
- 65 R. Ocampo-Perez, E. Padilla-Ortega, N. Medellin-Castillo, P. Coronado-Oyarvide, C. Aguilar-Madera, S. Segovia-Sandoval, R. Flores-Ramírez and A. Parra-Marfil, Synthesis of biochar from chili seeds and its application to remove ibuprofen from water. Equilibrium and 3D modeling, *Sci. Total Environ.*, 2019, **655**, 1397–1408.
- 66 A. Mojiri, R. Andasht Kazeroon and A. Gholami, Cross-Linked Magnetic Chitosan/Activated Biochar for Removal of Emerging Micropollutants from Water: Optimization by the Artificial Neural Network, *Water*, 2019, **11**, 551.
- 67 W. Phasuphan, N. Praphairaksit and A. Imyim, Removal of ibuprofen, diclofenac, and naproxen from water using chitosan-modified waste tire crumb rubber, *J. Mol. Liq.*, 2019, **294**, 111554.
- 68 L. Rafati, M. H. Ehrampoush, A. A. Rafati, M. Mokhtari and A. H. Mahvi, Removal of ibuprofen from aqueous solution by functionalized strong nano-clay composite adsorbent: kinetic and equilibrium isotherm studies, *Int. J. Environ. Sci. Technol.*, 2018, **15**, 513–524.
- 69 R. Manthiram Karthik and L. Philip, Sorption of pharmaceutical compounds and nutrients by various porous low cost adsorbents, *J. Environ. Chem. Eng.*, 2021, **9**, 104916.
- 70 O. I. Sahin, B. Saygi-Yalcin and D. Saloglu, Adsorption of ibuprofen from wastewater using activated carbon and graphene oxide embedded chitosan-PVA: equilibrium, kinetics, and thermodynamics and optimization with central composite design, *Desalin. Water Treat.*, 2020, **179**, 396–417.
- 71 Y. Liu, R. Liu, M. Li, F. Yu and C. He, Removal of pharmaceuticals by novel magnetic genipin-crosslinked chitosan/graphene oxide-SO<sub>3</sub>H composite, *Carbohydr. Polym.*, 2019, **220**, 141–148.

